Available online at www.sciencedirect.com
ScienceDirect
Trans. Nonferrous Met. Soc. China 25(2015) 759−769
Transactions of Nonferrous Metals Society of China
www.tnmsc.cn

Effect of thermo-mechanical processing on microstructure and electrochemical behavior of Ti−Nb−Zr−V new metastable β titanium biomedical alloy

Mohsin Talib MOHAMMED[1], Zahid A. KHAN[2], M. GEETHA[3]

1. Department of Mechanical Engineering, Faculty of Engineering, Kufa University, Najaf 54001, Iraq;
2. Department of Mechanical Engineering, Jamia Millia Islamia, New Delhi 110025, India;
3. Centre for Biomaterials Science and Technology, VIT University, Vellore 632014, India

Received 20 March 2014; accepted 2 September 2014

Abstract: The influence of thermo-mechanical processing (TMP) on the microstructure and the electrochemical behavior of new metastable β alloy Ti−20.6Nb−13.6Zr−0.5V (TNZV) was investigated. The TMP included hot working in below β transus, solution heat treatments at the same temperature and different cooling rates in addition to aging. Depending upon the TMP conditions, a wide range of microstructures with varying spatial distributions and morphologies of equiaxed/elongated α and β phases were attained, allowing for a wide range of electrochemical properties to be achieved. The corrosion behavior of the studied alloy was evaluated in a Ringer's solution at 37 °C via open circuit potential−time and potentiodynamic polarization measurements.

Key words: titanium alloy; thermo-mechanical processing; biomedical application; microstructure; electrochemical behavior; corrosion

1 Introduction

In the field of biomaterials, metallic implant materials such as stainless steels, cobalt−chromium based alloys and titanium (Ti) materials have made a significant impact in the latest decades especially in applications requiring electrochemical properties. Among metallic materials, Ti and its alloys are extensively used in a variety of applications like aerospace, chemical industries, power plants, and medical prostheses [1] due to their good mechanical properties and corrosion resistance [2]. They are considered the best choice for replacing or repairing failed hard tissues (structural biomedical applications) as these materials present excellent biocompatibility, high specific strength, outstanding corrosion resistance due to an oxide layer formation on the surface as well as low modulus of elasticity that is closer to bones than biomedical stainless steels and cobalt−chromium alloys, decreasing risk of catastrophic failure during prostheses service life [1−6].

Commercial pure Ti (CP) (ASTM F-67, ISO 5832-2) and Ti−6Al−4V (ASTM F-1472, ASTM F-136, ISO 5832-3) [7,8] are the most well known Ti materials used in biomedical applications. CP-Ti is used extensively in dental applications and found not to be suitable for load bearing applications owing to its poor mechanical properties such as low shear strength. The $\alpha+\beta$ type Ti–6Al–4V alloy has been used as structural biomaterial for manufacturing orthopedic prostheses as well as dental implants because of its excellent specific strength, corrosion resistance, and biocompatibility characteristics [9]. However, the alloying elements present in this alloy have their own adverse effect in biomedical environment. The literature also proves that the presence of vanadium (V) ions into human tissues can alter the kinetics of the enzyme activity associated with the inflammatory response cells [10,11]. Presence of aluminum (Al), on the other hand, increases the potential for the development of Alzheimer's disease [11−13] especially during long-term implantation.

Multifunctional β-type Ti alloys which are widely used in various biomedical applications have been developed all over the world. Recently, some new near β-type Ti alloys containing β-stabilizers such as Nb and Zr have attracted much special attention for orthopedic implant applications owing to their unique combination of better mechanical properties, low elastic modulus, superior biocorrosion resistance, nontoxicity against osteoblastic cells, no allergic problems, and excellent

Corresponding author: Mohsin Talib MOHAMMED; Tel/Fax: +91-11-26981259; E-mail: mohsent123@yahoo.com
DOI: 10.1016/S1003-6326(15)63661-5

biocompatibility. This type of Ti alloys exhibits extraordinary corrosion resistance in human body fluid. This behavior is due to the formation of a protective, hard and tightly adherent oxide film [14]. This oxide film offers chemical inertness to the Ti implants in human body fluid and guarantees its biocompatibility as a biomaterial. Therefore, Ti-based alloys with nontoxic and non-allergic elements such as Nb, Zr, and other elements have been widely used to design new β-type Ti alloys [15]. It is well known that Nb is β-stabilizer element and it forms homogenous solid solution with Ti in all kinds of Ti alloys when it is alloyed within certain concentration [16−18], while Zr is traditionally judged as a neutral element in the α- and α+β-type alloys. On the other hand, it is pointed out that Zr can be treated as a kind of β stabilizer in the Ti−Nb−Zr alloy system as this element can inhibit α precipitation according to TANG et al [19] and RIBERIO et al [20] and also reduce the martensitic transformation start temperature (M_s) considerably [21,22]. In this regard, the addition of Nb and Zr is preferable to developing absolutely safe Ti-based alloys for biomedical applications depending upon its ability to achieve biological passivity and capacity of reducing the elastic modulus [23].

In general, thermo-mechanical processing (TMP), a metallurgical process that integrates work hardening and heat treatment into a single process [24], plays a crucial role in producing a microstructure with outstanding properties in the materials [25−27]. The corrosion behavior [28] depends strongly on the alloy composition, processing history, heat treatment conditions which decide the varieties of microstructures. Near-β Ti alloys responding to thermal treatment and TMP and various microstructural constituents like the size, shape and the amount of the various phases can be modified by varying the TMP parameters. However, the influence of thermal treatment and TMP on microstructural features of as-cast Ti−Nb−Zr alloy system and in turn on its electrochemical behavior is scarcely reported. GEETHA et al [28] investigated the effect of heat treatment on the corrosion behavior of Ti−13Zr−13Nb alloy (ASTM F 1713-96) in Ringer's solution. They found that water-quenched α+β alloys possess superior corrosion resistance due to a homogeneous distribution of alloying elements. MAJUMDAR et al [29] studied the effect of TMP on the corrosion behavior of Ti−13Nb−13Zr alloy (TNZ) in simulated body fluid. It is found that the major results were mainly depending upon the cooling rate after solution treatment. The presence of larger amount of α phase in the microstructure showed lower corrosion potential (φ_{corr}) whereas the presence of α'' martensite and retained β phases caused further decrease in corrosion potential.

Nowadays, great efforts in terms of extensive work and focus are dedicated by engineers and materials scientists in developing novel Ti alloys for biomedical applications with superior electrochemical behavior. In this work, Ti−Ni−Zr-based alloy containing small amount of V was investigated in order to evaluate its possible application as a biomedical material. Nb, Zr and V, having a β-phase stabilizing effect for titanium materials, were chosen to control the microstructure desirably. The microstructure control was carried out by performing hot working in α+β phase field and subsequently heat treatment at the same temperature and different cooling rates. Finally, the relationship between thermomechanical processing and corrosion behavior was discussed in detail.

2 Experimental

The alloy in the present investigation was cast using the mixture of sponge Ti along with Ni powder and Zr chips as raw materials. The Ti−20.6Nb−13.6Zr−0.5V (TNZV) alloy was prepared using the non-consumable vacuum arc melting technique and supplied in the form of 600 g pancakes. The pancakes were re-melted three times to ensure compositional homogeneity. The composition of the alloy was analyzed and given in Table 1.

Table 1 Chemical composition of TNZV alloy used in this work (mass fraction, %)

Nb	Zr	V	Fe	Ti
20.6	13.6	0.5	0.14	Bal.

The as-cast TNZV alloy was then heat-treated at 1000 °C for 1 h for homogenization, and water cooled. Subsequently, the homogenized samples were given to 10% reduction by forging at below the β transition temperature (650 °C) and directly subjected to 25% reduction by rolling at the same temperature and then air cooled to room temperature. After entire plastic deformation, the alloy remained free from any of the metal working defects, which indicated that the entire metal working process was performed successfully.

The hot deformed TNZV samples were solution-treated at 650 °C (below β transus temperature) for 1 h in a dynamic argon atmosphere; this was followed by water quenching (WQ), air cooling (AC), or furnace cooling (FC). Aging treatment was done only on the water-quenched samples at 500 °C for 5 h. The TMP route of TNZV alloy is shown schematically in Fig. 1.

The compositions of the major and trace elements were determined using X-ray fluorescent (XRF) spectrometer (Oxford-X Srata, model: ISIS 1559). Microstructure analysis of the heat-treated samples was carried out using an optical microscope and field

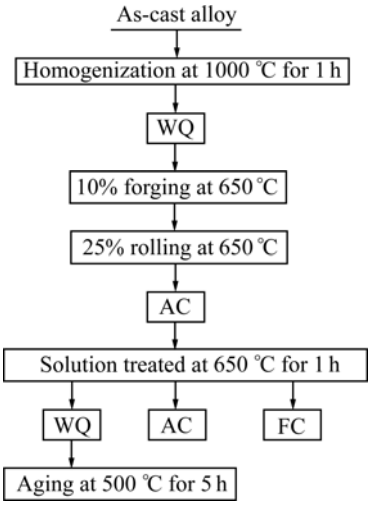

Fig. 1 Schematic diagram of thermo-mechanical processing of TNZV alloy

emission scanning electron microscope (FE-SEM, NOVA NANO SEM 450 FEI, Netherlands) at 2 kV. For this, the metallographic samples were prepared using standard techniques for Ti and its alloys [30]. They were ground to 1200 grit with silicon carbide (SiC), followed by final polishing to a mirror finish using 0.5 μm diamond paste. The metallographically polished samples were etched with Kroll's reagent (10% HF and 5% HNO_3 in water, volume fraction). Room temperature X-ray diffraction analysis was carried out on an X-ray diffractometer (Philips, Holland, PW 1830) with CuK_α radiation (wavelength 1.54056 Å) at an accelerating voltage of 40 kV and a current of 30 mA.

Vickers microhardness measurements were performed using a computer controlled precision microhardness tester (MicroWhizHard, Mitutoyo, Japan) with an indentation load of 3 N and a dwell time of 5 s for each of the indents. Ten indentations were taken for each specimen and the average values were considered. Hardness measurements were carried out on the samples finished using 0.5 μm diamond paste.

Tensile testing was performed as per ASTM E−8M standard to determine the ultimate tensile strength (UTS, σ_b), 0.2% offset yield strength ($\sigma_{0.2}$) and elongation (ε) using a conventional tensile testing unit (computerized FIE make universal testing machine, UTE−60), with a constant cross-head speed of 1 mm/min in air at room temperature. Dog-bone-shaped tensile specimens with dimensions as shown in Fig. 2 were precisely machined using wire electrical discharge machine (Wire-EDM). After machining, tensile specimens were polished using SiC water-proof papers of up to 2500 grit and the gage length of the specimens was mechanically polished using a diamond paste with a particle size 0.5 μm.

The corrosion behavior of the TNZV alloy was

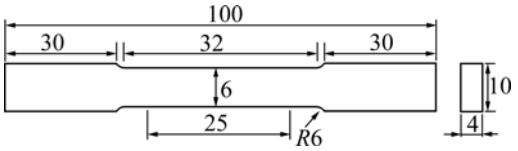

Fig. 2 Dimensions of tensile specimen proportional to ASTM E−8M standard (mm)

studied using potentiostat comprising of three-electrode cell with an Ag/AgCl (KCl saturated) as the reference electrode (all the potential measurements were made with reference to it) and a platinum foil as the counter electrode (cathode). The test specimens with dimensions of 10 mm×10 mm×2 mm were served as a working electrode (anode). Anodic polarization was carried out with a corrosion measuring system (model: WPG100e, Korea) which was computer interfaced through relevant software named Sequencer version 5. The open circuit potential (OCP) and passive current density were used as the criterion for evaluating the corrosion characteristics of the thermo-mechanically processed Ti alloy.

The surface area exposed to the electrolyte was 0.126 cm^2. For each experiment, the specimens were prepared by sequential grinding with water-proof emery paper up to 2000 grit SiC, followed by polishing with alumina of 0.5 μm for getting high mirror surface and then cleaning in an ultrasonic bath three times. Freshly prepared Ringer's solution was used as the electrolyte for each experiment to simulate physiological conditions representative of what a biomedical component would experience [1,31−33]. The solution had the following chemical composition dissolved in 1 L of distilled water: 9.00 g NaCl, 0.43 g KCl, 0.20 g $NaHCO_3$ and 0.24 g $CaCl_2$. The pH value of the solution was maintained at 7.4. The solution was naturally aerated and kept at (37±1) °C throughout the tests. Upon immersion of the specimens into the electrolyte, the open circuit potential (OCP) was measured as a function of time until the stable value was reached. Consequently, corrosion potential (φ_{corr}) and passive current density (J_{corr}) of the alloy were determined from the potential versus current density polarization curve. The polarization curves were obtained at a scan rate of 0.166 mV/s in the range from −750 to 2500 mV (vs Ag/AgCl). The polarization tests were repeated at least three times for each specimen. The corrosion potential (φ_{corr}) and corrosion current density (J_{corr}) were determined from the registered curves by the extrapolation method.

3 Results and discussion

3.1 Microstructure and XRD analysis

The present alloy which is called as "metastable-β-

alloy" subjected to thermomechanical processing exhibits various microstructures on heat treatment. Microstructure observations of the as-cast samples performed using optical microscopy (OM) and SEM show the presence of fine needle-like α phase (acicular α) in former β-phase matrix with segregation of α phase on grain boundaries (Figs. 3(a) and (b)). For each former β-grain, twelve different crystal orientations of the α precipitates (variants) are available according to the Burgers relationship [34], which links particular crystal directions and planes of both phases: $\langle 111\rangle_\beta // \langle 1120\rangle_\alpha$, $(110)_\beta // (0001)$.

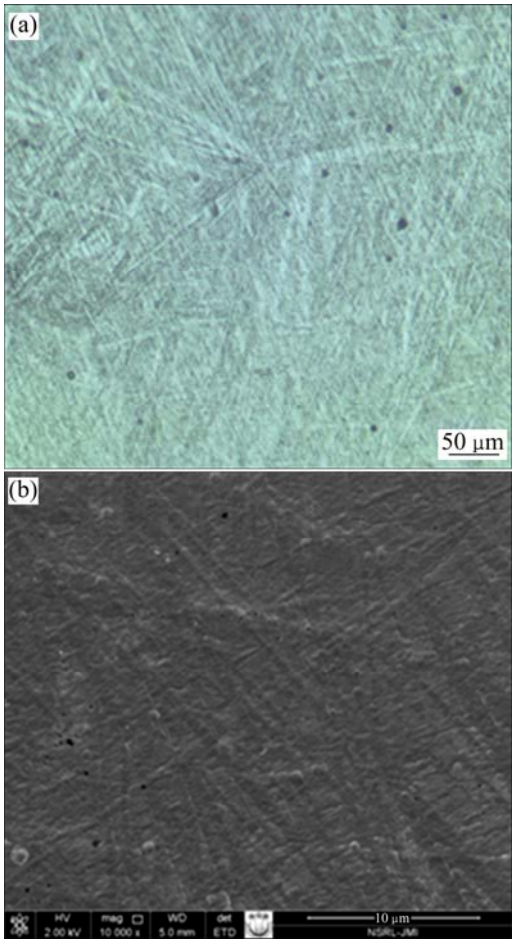

Fig. 3 Microstructures of as-cast TNZV alloy: (a) OM; (b) SEM

These phase constitutions were identified from XRD pattern, as shown in Fig. 4. XRD profiles revealed peaks corresponding to only α and β phases in the as-cast TNZV alloy.

The microstructure of an investigated TNZV alloy depends essentially upon both the plastic deformation process and heat treatment sequences imposed on it. In the present work, thermo-mechanical processing carried out by performing 10% forging plus 25% rolling at 650 °C (below β transus temperature) is a heavy deformation (>30%), which is an effective process to create worked structure in the alloy and nucleate α phase during the plastic deformation [35]. It is well known that the primary α phase (HCP) is one of the microstructural features in Ti alloys, which remains untransformed during solution treatment in the $\alpha+\beta$ phase field (650 °C). The thermo-mechanical processing plays an effective role in altering the morphology of primary α phase which can be lamellar, equiaxed or mixed [36]. It is expected that plastic deformation in the $\alpha+\beta$ field offers an extensive number of nucleation sites for the formation of α phase. At the same time, furnace cooling after solution treatment at 650 °C encourages the phase transformation of the β phase into α phase and forms a large number of α phase nucleation sites. Hence, subsequent solution treatment at 650 °C for a long holding time of 1 h followed by furnace cooling increases the volume fraction of α phase significantly and results in the recrystallization of any elongated α phase that may have formed during hot working at 650 °C. Consequently, the presence of primary equiaxed α phase and transformed β phase within pre-existing β phase is seen in the furnace-cooled (FC) samples solution-treated at 650 °C (Figs. 5(a) and 6(a)).

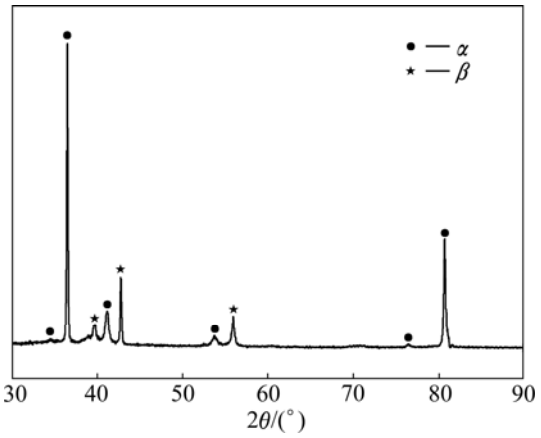

Fig. 4 XRD pattern of as-cast TNZV alloy

In the case of the air cooling (AC) after solution treatment at 650 °C, the microstructure consists of primary α phase and transformed β phase on a very fine scale. During this treatment, a part of the β phase transforms into α phase and large number of nucleation sites form, as shown in Figs. 5(b) and 6(b). It can be seen that all the furnace-cooled and air cooled TNZV samples consists of α and β phases. The samples subjected to deformation and solution treatment at 650 °C followed by water quenching (WQ) consists of fine scale elongated/globular α and retained β phase as matrix. Partial recrystallization of deformed α phase may happen owing to faster cooling (Figs. 5(c) and 6(c)). Many researches were reported [16,29,36,37−41] which confirmed the presence of martensite structure in

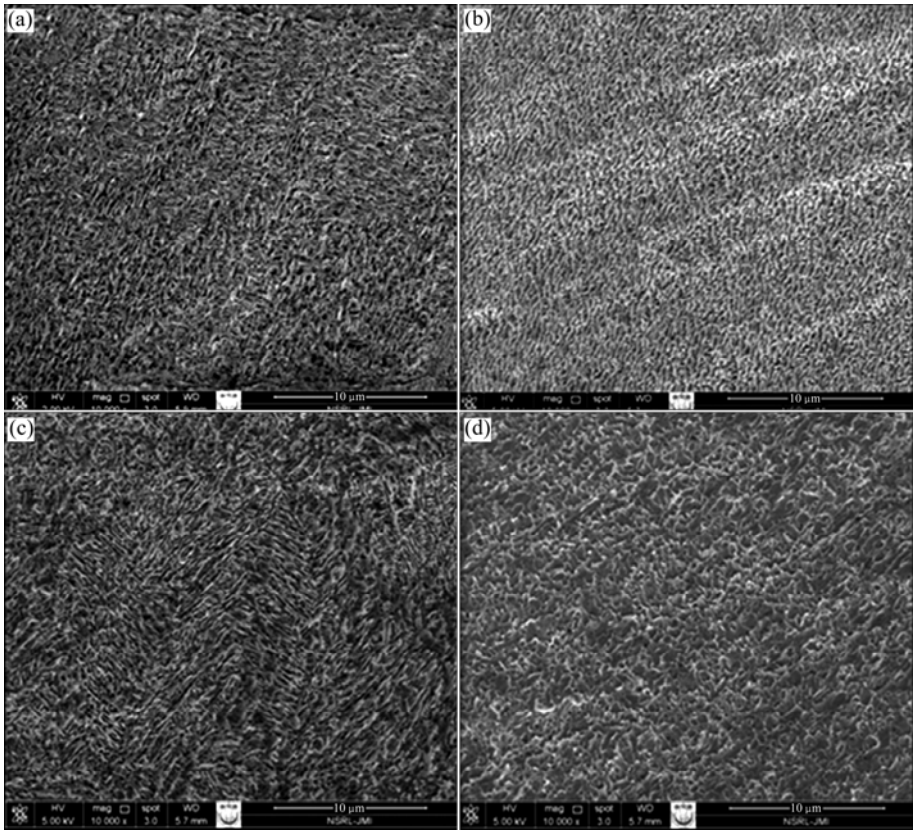

Fig. 5 SEM images (lower magnification) of TNZV alloy deformed at 650 °C and solution-treated at 650 °C for 1 h: (a) Furnace cooling; (b) Air cooling; (c) Water quenching; (d) Aging of WQ samples at 500 °C for 5 h

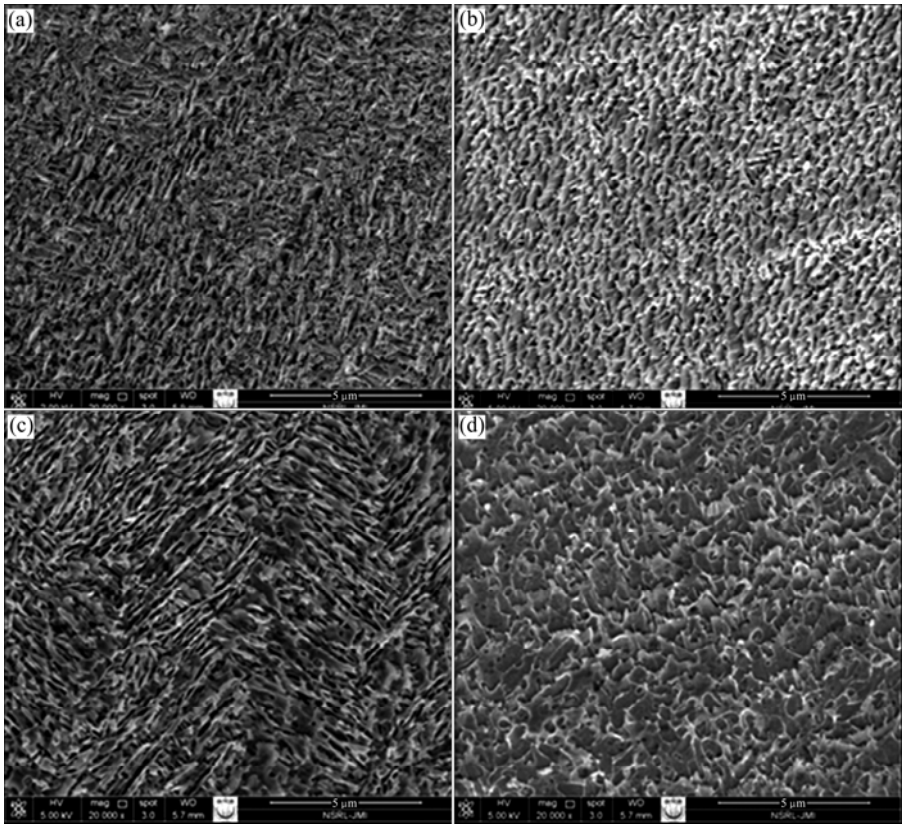

Fig. 6 SEM images (higher magnification) of TNZV alloy deformed at 650 °C and solution-treated at 650 °C for 1 h: (a) Furnace cooling; (b) Air cooling; (c) Water quenching; (d) Aging of WQ samples at 500 °C for 5 h

Ti materials if the solution treatment has been done at high temperature (above β phase field) with sufficiently high cooling rate. Hence, it is impossible here to produce martensite phase in the microstructure after fast cooling (WQ) from the below temperature (650 °C in this case). It was reported that partitioning of alloying elements occurred during solution treatment at below transus temperature along with β to α transformation [19,28]. Therefore, β phase becomes enriched with Nb and Zr elements during this treatment which reduces the martensite start temperature (M_s) of the untransformed β phase to below room temperature [19], and thus no martensite is created on water quenching from 650 °C.

The aging process of the WQ samples subjected to deformation and solution treatment at 650 °C established considerable growth of α from β phases (Figs. 5(d) and 6(d)). Moreover, aging modifies the morphology of the elongated α phase into equiaxed α phase.

The presence of different phases was further confirmed using the XRD patterns, as shown in Fig. 7. The peaks of α and β phases under all the heat-treated conditions were observed.

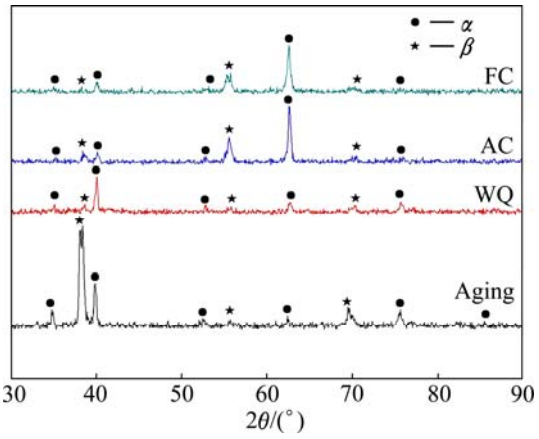

Fig. 7 XRD patterns of TNZV alloy deformed at 650 °C and solution-treated at 650 °C for 1 h followed by furnace cooling (FC), air cooling (AC), water quenching (WQ), and aging of WQ sample at 500 °C for 5 h

3.2 Electrochemical properties

3.2.1 Open circuit potential

Figure 8 represents the variation of open circuit potential (OCP) of TNZV alloy under different heat treatment conditions as a function of immersion time in naturally aerated Ringer's solution at 37 °C, until its variation with time becomes negligible. The steady state OCP of TNZV alloy varies with heat treatment conditions.

By comparing the results depicted in Fig. 8, it can be observed that the air-cooled samples present the most positive corrosion potential values (nobler behavior) compared with the furnace-cooled samples, water-

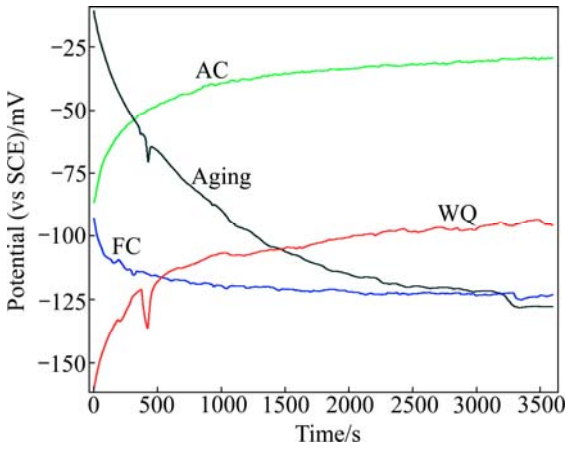

Fig. 8 Open circuit potential vs time curves in 37 °C Ringer's solution of TNZV alloy deformed at 650 °C and solution-treated at 650 °C for 1 h followed by furnace cooling (FC), air cooling (AC), water quenching (WQ) and aging of WQ sample at 500 °C for 5 h

quenched samples and also WQ plus aging samples. In the present work, among all the heat-treated samples, the furnace-cooled and aged samples show a substantial decrease in OCP. In addition, the OCP curves of WQ samples and aged WQ samples exhibit the fluctuation in the initial stage and then become stable. On the other hand, the AC and WQ samples show tendency of spontaneous formation of surface oxides and a continuous shifting towards noble (positive) direction when they are in contact with a Ringer's solution. It can be observed that the time profiles of the OCP are characteristic of passive film formation, especially in the stabilized region, on the alloy surfaces immersed in aerated solutions under different heat treatment conditions [42]. AC samples, however, display the greatest tendency to spontaneous oxide film formation in Ringer's solution. The OCP values for all heat treatment conditions show an overall increase for the time duration of 1 h, indicating that their corrosion resistance increases with the increase of time and reaches a relatively stable value. In other words, the OCP shifts in the positive direction, which indicates the formation of protective passive oxide film on the surface of the TNZV alloy.

The protective passive film forms rapidly and acts as a barrier for metal dissolution, thus reducing the corrosion rate. The thickness of the spontaneously formed protective oxide film on surfaces of Ti and its alloys has been reported as 1−4 nm under open circuit conditions [43]. It is well known that the superior corrosion behavior of Ti and its alloys is caused by the spontaneous creation of a tightly adherent protective oxide film on their surface even in solutions with low oxygen contents [44]. OLIVEIRA et al [45] reported an instance of an oxide film creation on Ti−13Zr−13Nb and

Ti−50Zr alloys in aerated solution. It was reported in the literature that X-ray photo-electron spectroscopy (XPS) revealed that the formed amorphous oxide film mainly consisted of TiO_2 [46] in addition to two types of oxides: TiO and Ti_2O_3, [14,47,48]. It has also been found that the oxides of titanium, TiO or Ti_2O_3, transform to more stable TiO_2 and come out on the electrode/electrolyte interface after a direct contact between Ti material and the electrolyte [22]. TiO_2 is an n-type semiconductor [49] and the corrosion of Ti is controlled kinetically by migration of oxygen vacancies through this film [50]. Hence, the corrosion behavior reached a relatively stable state as the corrosion resistance of the electrode was enhanced ultimately. The decrease of the anodic dissolution current of Ti alloy and shifting the OCP gradually in the positive direction are the normal results of corrosion resistance increase.

It is important to mention here that many researchers [43,51−53] found that the film formed on the surface of Ti and its alloys in various physiological solutions showed a two-layered structure comprising of a dense inner layer and a porous outer layer. The excellent corrosion behavior of the materials is essentially because of the barrier of inner layer which presents high resistance [42,51].

Many researchers [47,54−57] ensured that the passive film in Ti−Nb−Zr alloy system consisted principally of TiO_2 with a trace quantity of Nb_2O_5 and ZrO_2. The presence of Nb_2O_5 or ZrO_2 with the main passive TiO_2 layer developed the structural integrity of the oxide film and enhanced its resistance to dissolution [47,58]. For example, the presence of Nb cations enhanced the passivation properties of the surface film by decreasing the concentration of anion vacancies present on Ti oxide film. These anion vacancies were generated by the presence of lower Ti oxidation states [33,47,59]. ROBIN et al [42] proved through an electrochemical study that the high corrosion resistance of Ti−*x*Nb−13Zr alloy depended mainly on the resistance of the homogeneous barrier inner layer formed on the alloy in Ringer's solution at 37 °C. Moreover, it has also been pointed out that the inner layer formed on the surface of Ti−Nb−Zr alloy system is apparently more protective in comparison to other alloy systems as a result of the less porous passive film formed [51].

3.2.2 Potentiodynamic polarization

Figure 9 shows the potentiodynamic anodic polarization curves of different heat-treated TNZV samples as measured with respect to saturated calomel electrode (SCE) in naturally aerated Ringer's solution at 37 °C. The continuity, stability and intensity of the passive Ti oxide film were analyzed by this technique. As can be seen, the polarization curves obtained for the investigated TNZV alloy samples under all heat treatment conditions show a typical active–passive characterization, a rising anodic current with increasing potential and then transforming directly into the passive area from the Tafel curves. The passive current densities for the investigated TNZV alloy samples in all heat treatment conditions remain constant with increasing potential that reveals the thickening of their passive layer [60].

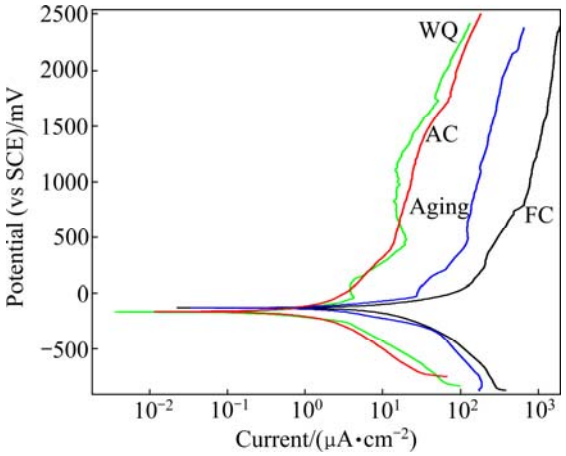

Fig. 9 Cyclic polarization behavior in 37 °C Ringer's solution of TNZV alloy deformed at 650 °C and solution-treated at 650 °C for 1 h followed by furnace cooling (FC), air cooling (AC), water quenching (WQ) and aging of WQ sample at 500 °C for 5 h

The average corrosion potentials (φ_{corr}) can be estimated from these curves as −133.97, −171.51, −171.64 and −137.74 mV (vs SCE) for the furnace-cooled samples, air-cooled samples, water-quenched samples and aged samples, respectively. The corrosion potentials determined from the polarization curves are significantly lower than those obtained from the open circuit potential measurements. This is expected, as the polarization tests started at a cathodic potential relatively to the corrosion potential, so that the surface passive oxide film was at least partially removed due to the highly reducing initial potentials.

The mean corrosion current densities (J_{corr}) and corrosion rates were obtained for investigated TNZV alloy by Tafel extrapolation analysis method using both anodic and cathodic branches of the polarization curves shown in Fig. 10.

The corresponding corrosion data which include the mean corrosion current densities (J_{corr}), corrosion potentials (φ_{corr}), and corrosion rates of TNZV alloy under different heat treatment conditions are given in Table 2.

From the above corrosion test results, it can be observed that in most of the heat treatment conditions, the corrosion potential (φ_{corr}) varies roughly within a narrow range. In general, air-cooled samples and water-

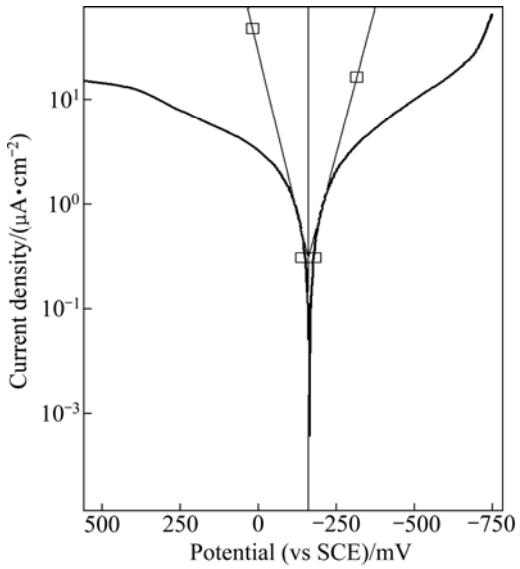

Fig. 10 Tafel plots obtained from furnace-cooled sample in Ringer's solution at 37 °C

Table 2 Results of electrochemical tests via anodic polarization curves of heat-treated TNZV alloy in Ringer's solution at 37 °C

Cooling condition	φ_{corr}/mV	J_{corr}/(μA·cm^{-2})	Corrosion rate/(μm·year^{-1})
FC	−133.97	12.8104	260
AC	−171.51	0.7983	16.25
WQ	−171.64	0.7776	15.75
Aging	−137.74	2.3685	47.5

quenched samples result further decrease in the φ_{corr} value and it is lower than that of the furnace-cooled samples and aged samples. The air-cooled samples and water-quenched samples show comparable φ_{corr} values whilst furnace-cooled and aged samples are also in almost analogous φ_{corr} values.

By comparing the four anodic curves, however, it can be noticed that the furnace-cooled samples and aged samples exhibit similar anodic polarization behaviors, including high current densities of 12.8104 and 2.3685 μA/cm^2 respectively at approximately 2.5 mV (vs SCE). On the other hand, the air-cooled samples and water-quenched samples shows comparable current densities of 0.7983 and 0.7776 μA/cm^2 respectively at approximately 2.5 mV (vs SCE).

As mentioned in OCP analysis, as soon as the TNZV samples are rinsed in the Ringer's solution, a protective surface oxide film is formed on the surface of samples and they get passivated, which is also reproduced in the anodic polarization curves (Fig. 9).

The furnace-cooled samples present the highest corrosion current density compared with air cooled and water-quenched samples. Moreover, the anodic current densities of air-cooled samples and water-quenched samples are lower than those of the furnace-cooled samples and aged samples. This indicates that among all the samples which are subjected to deformation and solution treatment at 650 °C, the minimum corrosion current density is observed in the case of air-cooled samples and water-cooled samples (Fig. 9) as the surface film formed on the air-cooled and water-quenched samples is more compact and protective. Consequently, this implies that the anodic current density of TNZV alloy in all heat treatment conditions increases with the increase in the potential, but this increase is always larger for the furnace-cooled and aged samples. The rise in current density with the potential is likely because of the insufficient increase in oxide film thickness with potential to re-compensate the increase in potential. It is reported that this current increase can be associated with the oxidation of TiO and Ti_2O_3 to TiO_2 [47]. Thus, it appears that the surface oxide films thicken to compensate the increase in potential where the current does not change with potential.

In the current research, it is expected that the fine $\alpha+\beta$ structure in the matrix of air-cooled samples increases the α/β interface area and then accelerates the galvanic corrosion of the alloy. Regardless of this, air-cooled samples show lower corrosion current density and corrosion rate compared with the furnace-cooled or aged-samples. It has been revealed that the corrosion behavior of CP-Ti (single α phase) is lower than that of Ti−6Al−7Nb alloy ($\alpha+\beta$) [61]. Therefore, the foremost reason of this better corrosion behavior of air-cooled samples is due to the small amount of less noble α phase in their microstructures. Further, the microstructure analysis of SEM (Figs. 5(c) and 6(c)) and XRD tests (Fig. 7) did not reveal any martensite formed in the water-quenched samples after solution treatment at 650 °C. The harmful corrosion behavior of the large amount of strain energy which is coupled with the martensite formation [62] will not happen as the microstructure consists of α and β phases only. Thus, no significant change in corrosion current density is found in air-cooled and water-quenched samples. The water-quenched samples have improved corrosion stability (lower J_{corr}) as a result of the formation of a more stable passive film than furnace-cooled or aged samples owing to the less amount of less noble phase (α) in the microstructure.

The researches related the better corrosion behavior of the Ti−Nb−Zr alloy system when Nb_2O_3 and ZrO_2 were represented in passive inner TiO_2 layer which worked as inhibitor to adsorption of Cl^- ions into the

oxide film and in turn increased the structural integrity of the oxide film [45,52]. Also, ROBIN et al [42] proved that the resistance of a compact oxide film formed on the Ti−13Nb−13Zr alloy is higher than that measured for Ti−6Al−4V alloy. This inference is derived from the fact that the presence of alloying elements in the Ti materials encourages the creation of ions like Nb^{5+} that increase the number of oxygen ions and cancel out the anion vacancies which make the film more stable and protective [59].

Aging treatment of water-quenched samples creates larger amounts of precipitates of less noble α phase in the microstructure as some part of the retained β phase transforms into α phase (Figs. 5(d) and 6(d)). Thus, in the same way, the α/β interface increases with the increase of α phase volume fraction which in turn leads to an increase in corrosion current density (J_{corr}) from 0.7776 to 2.3685 μA/cm^2.

4 Conclusions

1) The microstructure of the thermo-mechanical treated TNZV alloy consists mainly of equiaxed/ elongated α and β phases with different morphologies depending upon the heat treatment conditions.

2) Corrosion tests indicate that TNZV alloy undergoes spontaneous passivation owing to spontaneously formed oxide film in the human body environment.

3) The air-cooled and water-quenched samples show lower corrosion rate owing to the less amount of noble phase α in the microstructure.

Acknowledgments

Mohsin Talib MOHAMMED would like to sincerely acknowledge the financial assistance provided by Ministry of High Education and Scientific Research, the Government of Iraq. He would also like to thank the Iraqi Cultural Office, New Delhi, India and Indian Council of Cultural Relations (ICCR), New Delhi, India for supporting him during the period of his PhD program. Many thanks to Defense Metallurgical and Research Laboratories—Hyderabad, India, for helping us with manufacturing cast Ti alloy.

References

[1] CREMASCO A, OSORIO W R, FREIRE C M A, GARCIA A, CARAM R. Electrochemical corrosion behaviour of a Ti−35Nb alloy for medical prostheses [J]. Electrochim Acta, 2008, 53: 4867−4874.

[2] LONG M, RACK H J. Titanium alloys in total joint replacement—A materials science perspective [J]. Biomaterials, 1998, 19: 1621−1639.

[3] WANG K. The use of titanium for medical applications in the USA [J]. Mater Sci Eng A, 1996, 213: 134−137.

[4] BOEHLERT C J. Microstructure, creep, and tensile behavior of a Ti−12Al−38Nb (at.%) beta and orthorhombic alloy [J]. Mater Sci Eng A, 1999, 267: 82−98.

[5] NIINOMI M. Recent research and development in titanium alloys for biomedical applications and healthcare goods [J]. Science and Technology of Advanced Materials, 2003, 4: 445−454.

[6] MYTHILI R, THOMAS PAUL V, SAROJA S, VIJAYALAKSHMI M, RAGHUNATHAN V S. Study of transformation behavior in Ti−4.4Ta−1.9Nb alloy [J]. Mater Sci Eng A, 2005, 390: 299−312.

[7] HANAWA T. Recent development of new alloys for biomedical use [J]. Mater Sci Forum, 2006, 512: 243−247.

[8] BROJAN D, FAJFAR P, KOSEL F, TURK R. Review of materials in medical applications [J]. RMZ Mater Geoenviron, 2007, 54: 471−479.

[9] NIINOMI M. Fatigue performance and cyto-toxicity of low rigidity titanium alloy, Ti−29Nb−13Ta−4.6Zr [J]. Biomaterials, 2003, 24(16): 2673−2683.

[10] YU J, ZHAO Z J, LI L X. Corrosion fatigue resistances of surgical implant stainless steel and titanium alloys [J]. Corros Sci, 1993, 35: 587−597.

[11] OKAZAKI Y, ITO Y, KYO K, TATEISHI T. Corrosion resistance and corrosion fatigue strength of new titanium alloys for medical implants without V and Al [J]. Mater Sci Eng A, 1996, 213: 138−147.

[12] RAO S, OKAZAKI Y, TATEISHI T, USHIDA T, ITO Y. Cytocompatibility of new Ti alloy without Al and V by evaluating the relative growth ratios of fibroblasts L929 and osteoblasts MC3T3-E1cells [J]. Mater Sci Eng C, 1997, 4: 311−316.

[13] IKEDA M, KOMATSU SY, SOWA I, NIINOMI M. The effect of tantalum content on phase constitution and aging behaviour of Ti−Ta binary alloys [J]. Metall Mater Trans, 2002, 33: 487−491.

[14] BEEN J, GRAUMAN J S. Titanium and titanium alloys [M]. New York: John & Wiley, Inc., 2000.

[15] NIINOMI M. Mechanical properties of biomedical titanium alloys [J]. Mater Sci Eng A, 1998, 243: 231−236.

[16] COLLINGS E W. Physical metallurgy of titanium alloys [M]. OH: ASM International, 1984.

[17] NIINOMI M, AKAHORI T, TAKEUCHI T, KATSURA S, FUKUI H, TODA H. Mechanical properties and cyto-toxicity of new beta type titanium alloy with low melting points for dental applications [J]. Mater Sci Eng C, 2005, 25: 417−425.

[18] ZHANG R G, ACOFF V L. Processing sheet materials by accumulative roll bonding and reaction annealing from Ti/Al/Nb elemental foils [J]. Mater Sci Eng A, 2007, 463: 67−73.

[19] TANG X, AHMED T, RACK H J. Phase transformations in Ti−Nb−Ta and Ti−Nb−Ta−Zr alloys [J]. J Mater Sci, 2000, 35: 1805−1811.

[20] RIBEIRO A L R, RUBENS C J, FLÁVIA F C, ROMEU B F F, LUIS GERALDO V. Mechanical, physical, and chemical characterization of Ti−35Nb−5Zr and Ti−35Nb−10Zr casting alloys [J]. J Mater Sci: Mater Med, 2009, 20: 1629−1636.

[21] KIM J I, KIM H Y, INAMURA T, HOSODA H, MIYAZAKI S. Shape memory characteristics of Ti−22Nb−(2−8)Zr(at.%) biomedical alloys [J]. Mat Sci Eng A, 2005, 403: 334−339.

[22] SUN F, HAO Y L, NOWAK S, GLORIANT T, LAHEURTE P, PRIMA F. A thermo-mechanical treatment to improve the superelastic performances of biomedical Ti−26Nb and Ti−20Nb−6Zr (at.%) alloys [J]. J Mech Behav Biomed Mater, 2011, 4: 1864−1872.

[23] YANG G, ZHANG T. Phase transformation and mechanical

properties of the $Ti_{50}Zr_{30}Nb_{10}Ta_{10}$ alloy with low modulus and biocompatible [J]. J Alloys Compd, 2005, 392: 291−294.

[24] DEGARMO PAUL E, BLACK J T, KOHSER RONALD A. Materials and processes in manufacturing [M]. New York: John Wiley & Sons, 2003.

[25] WEAVER M L, GARMESTANI H. Microstructures and mechanical properties of commercial titanium foils processed via the melt overflow process [J]. Mater Sci Eng A, 1998, 247: 229−238.

[26] BACHE M R, EVANS W J. Impact of texture on mechanical properties in an advanced titanium alloy [J]. Mater Sci Eng A, 2001, 319−321: 409−414.

[27] LONARDELLI I, GEY N, WENK H R, HUMBERT M, VOGEL S C, LUTTEROTTI L. In situ observation of texture evolution during $\alpha\rightarrow\beta$ and $\beta\rightarrow\alpha$ phase transformations in titanium alloys investigated by neutron diffraction [J]. Acta Mater, 2007, 55: 5718−5727.

[28] GEETHA M, MUDALI U K, GOGIA A K, ASOKAMANI R, BALDEV R. Influence of microstructure and alloying elements on corrosion behavior of Ti−13Nb−13Zr alloy [J]. Corros Sci, 2004, 46: 877−892.

[29] MAJUMDAR P, SINGH S B, CHATTERJEE U K, CHAKRABORTY M. Corrosion behaviour of heat treated boron free and boron containing Ti−13Zr−13Nb (wt%) alloy in simulated body fluid [J]. J Mater Sci: Mater Med, 2011, 22: 797−807.

[30] KUHN H, MEDLIN D. Metals handbook (Vol.8): Mechanical testing and evaluation [M]. OH: ASM International, 1972.

[31] GONZALEZ J E G, MIRZA-ROSCA J C. Study of the corrosion behaviour of titanium and some of its alloys for biomedical and dental applications [J]. J Electroanal Chem, 1999, 471: 109−112.

[32] OLIVEIRA N T C, BIAGGIO S R, ROCHA-FILHO R C, BOCCHI N. Electrochemical studies on zirconium and its biocompatible alloys Ti−50Zr at.% and Zr−2.5Nb wt% in simulated physiologic media [J]. J Biomed Mater Res, 2005, 74: 397−407.

[33] ROSALBINO F, MACCIÓD, SCAVINO G, SACCONE A. In vitro corrosion behaviour of Ti−Nb−Sn shape memory alloys in Ringer's physiological solution [J]. J Mater Sci: Mater Med, 2012, 23: 865−871.

[34] BURGERS W. On the process of transition of the cubic-body-centered modification into the hexagonal-close-packed modification of zirconium [J]. Physica, 1934, 1: 561−586.

[35] MAJUMDAR P, SINGH S B, CHAKRABORTY M. The role of heat treatment on microstructure and mechanical properties of Ti−13Zr−13Nb alloy for biomedical load bearing applications [J]. J Mech Behav Biomed Mater, 2011, 4: 1132−1144.

[36] BOYER R, WELSCH G, COLLINGS E W. Materials properties handbook: Titanium alloys [M]. OH: ASM International, 1994.

[37] AHMED T, RACK H J. Martensitic transformations in Ti−(16−26at%)Nb alloys [J]. J Mater Sci, 1996, 31: 4267−4276.

[38] HAO Y L, NIINOMI M, KURODA D, FUKUNAGA K, ZHOU Y L, YANG R, SUZUKI A. Young's modulus and mechanical properties of Ti−29Nb−13Ta−4.6Zr in relation to α'' martensite [J]. Metallurgical and Materials Transactions A, 2002, 33: 3137−3144.

[39] MANTANI Y, TAJIMA M. Phase transformation of quenched α'' martensite by aging in Ti−Nb alloys [J]. Mater Sci Eng A, 2006, 438−440: 315−319.

[40] BANUMATHY S, PRASAD K S, MANDAL R K, SINGH A K. Effect of thermomechanical processing on evolution of various phases in Ti−Nb alloys [J]. Bull Mater Sci, 2011, 34: 1421−1434.

[41] LEE T, HEO Y U, LEE C S. Microstructure tailoring to enhance strength and ductility in Ti−13Nb−13Zr for biomedical application [J]. Scripta Materialia, 2013, 69: 785−788.

[42] ROBIN A, CARVALHO O A S, SCHNEIDER S G, SCHNEIDER S. Corrosion behavior of Ti−xNb−13Zr alloys in Ringer's solution [J]. Mater Corros, 2008, 59: 929−933.

[43] MARINO C E B, OLIVEIRA E M, ROCHA-FILHO R C, BIAGGIO S R. On the stability of thin-anodic-oxide films of titanium in acid phosphoric media [J]. Corros Sci, 2001, 43: 1465−1476.

[44] OKAZAKI Y, TATEISHI T, ITO Y. Corrosion resistance of implants alloys in pseudo physiological solution and role of alloying elements in passive films [J]. Mater Trans JIM, 1997, 38: 78−84.

[45] OLIVEIRA N T C, FERREIRA E A, DUARTE L T, BIAGGIO S R, ROCHA-FILHO R C, BOCCHI N. Corrosion resistance of anodic oxides on the Ti−50Zr and Ti−13Zr−13Nb alloys [J]. Electrochim Acta, 2006, 51: 2068−2075.

[46] NARAYANAN R, SESHADRI S K. Point defect model and corrosion of anodic oxide coatings on Ti−6Al−4V [J]. Corros Sci, 2008, 50: 1521−1529.

[47] YU S Y, SCULLY J R. Corrosion and passivity of Ti−13Nb−13Zr in comparison to other biomedical implant alloys [J]. Corrosion, 1997, 53: 965−976.

[48] POUILLEAU J, DEVILLIERS D, GARRIDO F, DURAND-VIDAL S, MAHÉ E. Structure and composition of passive titanium oxide films [J]. Mater Sci Eng B, 1997, 47: 235−243.

[49] PAN J, LEYGRAF C, THIERRY D, EKTESSABI A M. Corrosion resistance for biomaterial applications of TiO_2 films deposited on titanium and stainless steel by ion-beam-assisted sputtering [J]. J Biomed Mater Res, 1997, 35: 309−318.

[50] HONG S B, ELIAZ N, SACHS E M, ALLEN S M L. Corrosion behavior of advanced titanium-based alloys made by three-dimensional printing (3DP^{TM}) for biomedical applications [J]. Corros Sci, 2001, 43: 1781−1791.

[51] ASSIS S L, COSTA I. Electrochemical evaluation of Ti−13Nb−13Zr, Ti−6Al−4V and Ti−6Al−7Nb alloys for biomedical application by long-term immersion tests [J]. Mater Corros, 2007, 58: 329−333.

[52] ASSIS S L, WOLYNEC S, COSTA I. The electrochemical behaviour of Ti−13Nb−13Zr alloy in various solutions [J]. Mater Corros, 2008, 59: 739−743.

[53] ALVES V A, REIS R Q, SANTOS I C B, SOUZA D G, de GONCALVES T F, PEREIRA-DA-SILVA M A, ROSSI A, da SILVA L A. In situ impendance spectroscopy study of the electrochemical corrosion of Ti and Ti−6Al−4V in simulated body fluid at 25 °C and 37 °C [J]. Corros Sci, 2009, 51: 2473−2482.

[54] MANIVASAGAM G, MUDALI U K, ASOKAMANI R, RAJ B. Corrosion and microstructural aspects of titanium and its alloys as orthopaedic devices [J]. Corros Rev, 2003, 21: 125−159.

[55] CHOUBEY A, BASU B, BALASUBRAMANIAM R. Electrochemical behavior of Ti based alloys in simulated human body fluid environment [J]. Trends Biomater Artif Organs, 2005, 18: 64−72.

[56] LI J, ZHOU L, LI Z. Corrosion behavior of a new titanium alloy TZNT for surgical implant application in Ringer's solution [J]. Rare Metals, 2010, 29: 37−44.

[57] BAI Y LI S J, PRIMA F, HAO Y L, YANG R. Electrochemical corrosion behavior of Ti−24Nb−4Zr−8Sn alloy in a simulated physiological environment [J]. Applied Surface Science, 2012, 258: 4035−4040.

[58] GEETHA M, SINGH A K, ASOKAMANI R, GOGIA A K. Ti based biomaterials, the ultimate choice for orthopaedic implants—A review [J]. Prog Mater Sci, 2009, 54: 397−425.

[59] METIKOŠ-HUKOVIĆ M, KWOKAL A, PILJAC J. The influence of niobium and vanadium on passivity of titanium-based implants in physiological solution [J]. Biomaterials, 2003, 24: 3765−3775.

[60] KARTHEGA M, RAMAN V, RAJENDRAN N. Influence of

potential on the electrochemical behaviour of β titanium alloys in Hank's solution [J]. Acta Biomater, 2007, 3: 1019−1023.

[61] RAMAN V, TAMILSELVI S, NANJUNDAN S, RAJENDRAN N. Electrochemical behaviour of titanium and titanium alloy in artificial saliva [J]. Trends Biomater Artif Organs, 2005, 18: 137−140.

[62] WAYMAN C M, BHADESHIA H K D H. Phase transformations, nondifusive. Physical metallurgy [M]. Amsterdam: Elsevier Science Publishers, 1996.

机械热处理对新型亚稳态β钛生物合金显微组织和电化学行为的影响

Mohsin Talib MOHAMMED[1], Zahid A. KHAN[2], M. GEETHA[3]

1. Department of Mechanical Engineering, Faculty of Engineering, Kufa University, Najaf 54001, Iraq;
2. Department of Mechanical Engineering, Jamia Millia Islamia, New Delhi 110025, India;
3. Centre for Biomaterials Science and Technology, VIT University, Vellore 632014, India

摘　要：研究机械热处理对新型亚稳态β钛生物合金显微组织和电化学行为的影响。机械热处理方法包括在β相转变温度下热加工处理及在相同温度固溶热处理，经不同冷却速率冷却后进行时效处理。在不同的机械热处理条件下获得具不同空间分布和等轴/拉长α和β相形貌的合金组织。这些合金组织具有不同的电化学性能。通过开路电位和动电位极化测试方法，测定合金在37 ℃ NaCl溶液(林格氏试剂)中的腐蚀行为。

关键词：钛合金；机械热处理；生物医学应用；显微组织；电化学性能；腐蚀

(Edited by Wei-ping CHEN)